UNIVERSAL POWER FILTER WITH PHOTOVOLTAIC CO-GENERATION FOR SINGLE-PHASE SYSTEMS

Welflen R. N. Santos*, Montiê A. Vitorino*, Lucas V. Hartmann*, Maurício B. R. Corrêa*, Cursino B. Jacobina*, Edison R. C. da Silva*, Alexandre C. Oliveira*
*Unidade Acadêmica de Engenharia Elétrica
Universidade Federal de Campina Grande (UFCG-PB)
58.109-970 Av. Aprígio Veloso, 882
Campina Grande - Paraíba, Brasil
Emails: welflen@dee.ufcg.edu.br, montie.vitorino@ee.ufcg.edu.br, lucas.hartmann@ee.ufcg.edu.br, mbrcorrea@dee.ufcg.edu.br, jacobina@dee.ufcg.edu.br, edison@dee.ufcg.edu.br, aco@dee.ufcg.edu.br

***Abstract*— This paper presents a photovoltaic generator integrated to a single-phase universal power filter based on a single-phase four-leg converter. The topology and its operating principles are presented. A suitable control strategy is proposed to improve the use of the topology when disturbances occur in the voltage source. Simulated and experimental results are presented.**

***Keywords*— MPPT, Photovoltaic, Universal Power Filter.**

I. INTRODUCTION

Strict regulations about the flow of electrical energy have stimulated the use of active power compensation schemes [1, 2]. The active power compensation is normally achieved with the help of switching converters connected as an active filter to the load and the grid. An universal power filter provides simultaneously voltage and power factor control. A series-active filter may eliminate voltage disturbances, such as sag, notch, flicker and unbalance. The purpose of a shunt-active filter is to absorb current harmonics, compensate for reactive power and negative sequence current, and regulate the dc-bus voltage between both active filters.

Lately, renewable energy sources have also been focused [3], wind- and solar-powered generators getting most of attention. Wind turbines are installed on the top of special towers, taking a considerable area which is not usually shared with other applications. Noise may also be an issue, as the turbines can be heard from a few hundred meters in distance. On the other hand, photovoltaic (PV) generators can be easily installed on rooftops and make no noise at all, while the absence of moving parts reduces the maintenance costs. Recently developed semi-transparent models are also being used as light filters on the façade of commercial buildings [4]. However, the output power from a photovoltaic generator is a direct-current (DC) signal, therefore requiring appropriate handling before it can be connected to the electrical grid.

This paper presents a PV generator using a push-pull converter to feed power to the DC bus of a four-legged single-phase universal power filter as shown in Fig. 1, in which e_s is the grid voltage, Z_s is the grid impedance, i_s is the grid current, v_{ca} is the capacitor voltage, Z_{lt} is the impedance of the transmission line, e_l is the load voltage, Z_l is the load impedance, i_l is the load current, Z_g is the G converter's input impedance, i_g is the G converter's input current, v_g is the G converter's voltage, Z_f is the F converter's output impedance, i_f is the F converter's output current, v_f is the F converter's voltage, Z_a and Z_b are respectively the a and b impedances of transformer, m_{ab} is the mutual inductance of transformer, E is the DC bus voltage, v_p is the PV generator's voltage, i_p is the PV generator current, C_i is the push-pull input capacitor, L_i is the push-pull inductor, and L_p and L_s are the primary and secondary inductances of the push-pull transformer.

The filter is then used to handle the power appropriately and feed it to the grid. Simulation and experimental results are presented for the universal power filter, as for the complete system simulation results are presented.

II. PHOTOVOLTAIC GENERATOR

The PV generators are usually constituted by several cells, where a cell is a thin silicon piece with two faces around 30-100cm^2 in area. The faces of the cell are doped as P and N, forming a junction similar to a diode. With the N face exposed to the sunlight, the photoelectric effect creates several free-electrons on the N face, and as these cross over the junction a voltage drop around 0.65V is created. The number of free electrons, and therefore the current circulating, is directly proportional to the surface area of the cell and the incident sunlight. With an insolation of $1000W/m^2$ and appropriate control, the power generated is typically around $140W/m^2$ of the silicon surface.

A. Model of the Photovoltaic Generator

A solar cell may be described by the circuit shown in Fig. 2 [5]. The photoelectric current is described by I_{ph}, the P-N junction behavior is described by the diode, and the parasitic losses are described by the resistances R_S and R_P.

For this circuit, the output current I is given by (1), where I_D and I_R are function of the voltage over I_{ph}. Replacing I_D and I_R accordingly, the mathematical representation of the discrete components yields (2).

$$I = I_{ph} - I_D - I_R \quad (1)$$

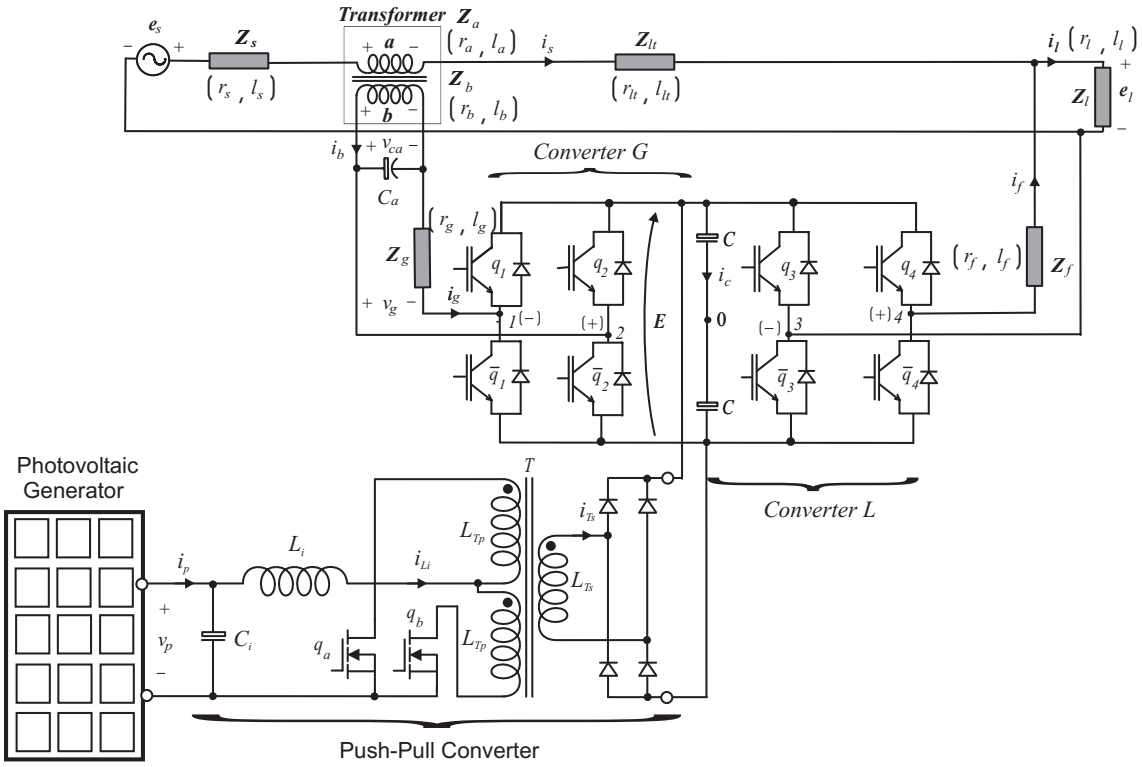

Fig. 1: Single-phase universal power filter with photovoltaic co-generator

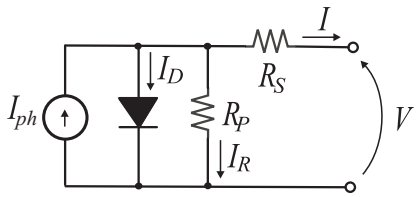

Fig. 2: Circuit model of photovoltaic generator

$$I = I_{ph} - I_O \left(\exp\left(\frac{V + R_S I}{m V_t} \right) - 1 \right) - \frac{V + R_S I}{R_P} \quad (2)$$

where I_O is the diode's reverse saturation current, V is the output terminal voltage, m is the ideality factor of the diode, $V_t = kT/q$ is the thermal potential, $k = 1.38 \cdot 10^{-23} J/K$ is the Boltzman's constant, $q = 1.6 \cdot 10^{-19} C$ is the electron's charge, and T is the temperature expressed in Kelvin.

Equation (2) describes the characteristic curve of the PV generator and a sample plot of this is shown in Fig. 3 along with the output power generated $P = VI$. The short-circuit current I^r_{SC}, the open-circuit voltage V^r_{OC}, the voltage for maximum power V^r_{max} and the current for maximum power I^r_{max} are parameters available from the generator manufacturer. The ^{r} indexes stand for values measured under reference conditions for insolation ($G^r = 1000 W/m^2$) and temperature ($T^r = 298.16 K$).

Temperature and insolation have direct influence on the cell's operation. This influence is described by (3) and (4), where $m' = m/N_{sm}$ is the equivalent ideality factor

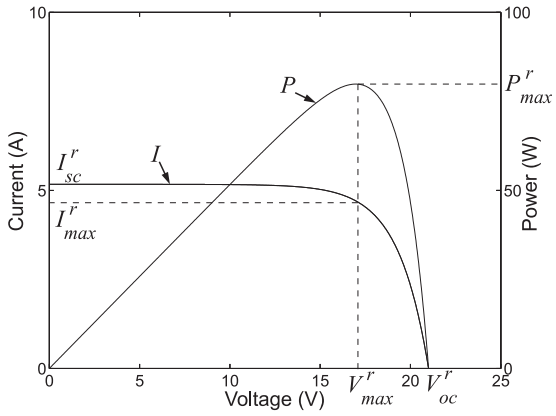

Fig. 3: Characteristic curve

and N_{sm} is the number of cells connected in series.

$$I_{ph} = I^r_{ph} \frac{G}{G^r} \quad (3)$$

$$I_O = I^r_O \left(\frac{T}{T^r} \right)^3 \exp\left(\frac{\varepsilon}{m'} \left(\frac{1}{V^r_t} - \frac{1}{V_t} \right) \right) \quad (4)$$

B. *Maximum Power Point Tracking*

In Fig. 3, the presence of a point in which the output power of the generator is maximum may be easily noticed. This point is called the Maximum Power Point (MPP), and it's position changes under insolation and temperature variations. Several specialized algorithms were proposed for determination of MPP position [6], [7] and [8]; these are called MPP Trackers (MPPT).

The implementation of a MPPT algorithm requires a device capable of controlling the power flow from the generator to the load. In this paper a push-pull converter as shown in Fig. 1 is used for this purpose. The converter may control either the voltage or the current through the generator depending on the requirements of the algorithm.

In this paper the MPPT algorithm used is called Incremental Conductance (IncCond) [9], this algorithm uses the derivative (5) to determine wether P increases by V increasing or decreasing. Therefore, if $dP/dV > 0$ then V is increased by ΔV, if $dP/dV < 0$ then V is decreased by ΔV, otherwise V remains constant.

$$\frac{dP}{dV} = \frac{d[IV]}{dV} = I + V\frac{dI}{dV} = 0 \tag{5}$$

Equation (5) is checked for divide-by-zero errors and modified to a different computational form, resulting in the flowchart shown in Fig. 4 [9].

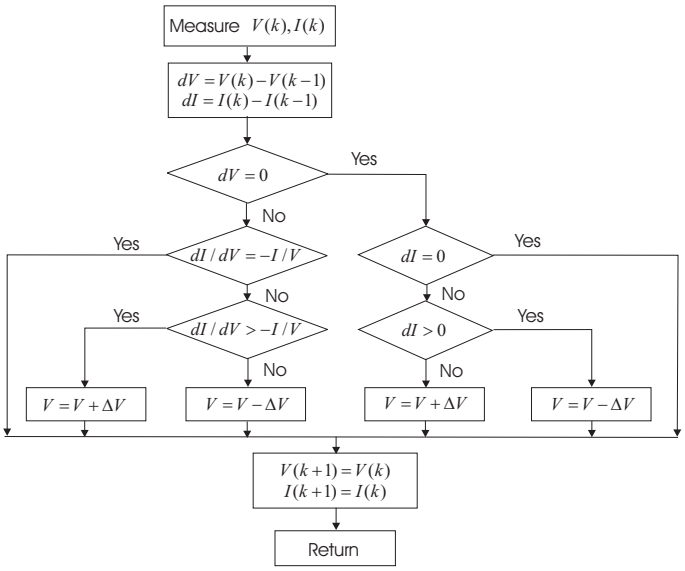

Fig. 4: Algorithm for the IncCond MPPT

III. PUSH-PULL CONVERTER

The push-pull converter is used to raise the voltage level of DC power, and to provide galvanic isolation between the PV generator and the universal filter. While both q_a and q_b are closed, as in Fig. 5(a), the PV generator transfers energy to the inductor L, and the filter's load is supplied by the energy stored on the capacitors C. While either q_a or q_b is open, as in Fig. 5(b) and Fig. 5(c), both the generator and the inductor transfer energy through the transformer to the filter's DC link capacitors C and the load.

The ratio between the period in which both switches are closed and the switching period is called duty cycle D, and may be used to control the converter operation. The duty cycle is always between 0 and 1 inclusive, but independently of his value the output voltage for this converter is always higher than the input voltage reflected to the secondary of the transformer.

Since in this paper the push-pull converter is connected to the PV generator, some more considerations arrive. It should be noticed that as D raises, the current through L and the generator raises as well. This will also cause a reduction on the generator's voltage, establishing a negative relation between D and V. This information is used replacing voltage increments with duty-cycle decrements and voltage decrements with duty-cycle increments, obtaining the implemented controller for the push-pull converter. Since this controller always delivers the maximum power available from the PV generator to the DC-bus, changes on environmental conditions will change the power delivered, acting as a disturbance on the DC-bus voltage. Insolation changes are, however, slow enough for the filter's voltage control loop to handle properly.

Simulation is performed by using the state-space equations (6), where q_a and q_b should be replaced by zero/one when the respective switch is open/closed, and ϕ_{Ts}, defined by (7), is the flux on the transformer core as seen from the secondary winding.

$$\begin{cases} \dot{I_{Li}} = \frac{V_p - \sqrt{L_{Tp}/L_{Ts}}V_o(1-q_a q_b)}{L_i} \\ \dot{V_p} = \frac{I_p - I_L i}{C_i} \\ \dot{\phi_{Ts}} = (q_b - q_a)\,E \end{cases} \tag{6}$$

$$\phi_{Ts} = \sqrt{L_{Tp}L_{Ts}}\,(I_{qb} - I_{qa}) - L_{Ts}i_{Ts} \tag{7}$$

IV. FILTER VOLTAGES

The basic scheme of AC/AC converter presented in this paper is shown in Fig. 1. The converter is comprised by four-legs (eight semiconductor power switches) and a capacitor bank at DC-bus. The converter G is composed by switches q_1, $\overline{q}_1$, q_2 and $\overline{q}_2$. The converter F is composed by switches q_3, $\overline{q}_3$, q_4 and $\overline{q}_4$. The conduction state of all switches can be represented by an homonymous binary variables q_1, $\overline{q}_1$, q_2, $\overline{q}_2$, q_3, $\overline{q}_3$, q_4 and $\overline{q}_4 \in \{0,1\}$, where $q = 1$ indicates a closed switch, while $q = 0$ indicates an open one. The pairs $q_1 - \overline{q}_1$, $q_2 - \overline{q}_2$, $q_3 - \overline{q}_3$ and $q_4 - \overline{q}_4$ are complementary and, therefore $\overline{q}_1 = 1 - q_1$, $\overline{q}_2 = 1 - q_2$, $\overline{q}_3 = 1 - q_3$ and $\overline{q}_4 = 1 - q_4$.

The converter poles voltages v_{10}, v_{20}, v_{30} and v_{40} depend on the states of the power switches and may be expressed in terms of the previously defined variables q_1, q_2, q_3 and q_4 as

$$v_{10} = (2q_1 - 1)\frac{E}{2} \tag{8}$$

$$v_{20} = (2q_2 - 1)\frac{E}{2} \tag{9}$$

$$v_{30} = (2q_3 - 1)\frac{E}{2} \tag{10}$$

$$v_{40} = (2q_4 - 1)\frac{E}{2} \tag{11}$$

where E is the DC-bus voltage.

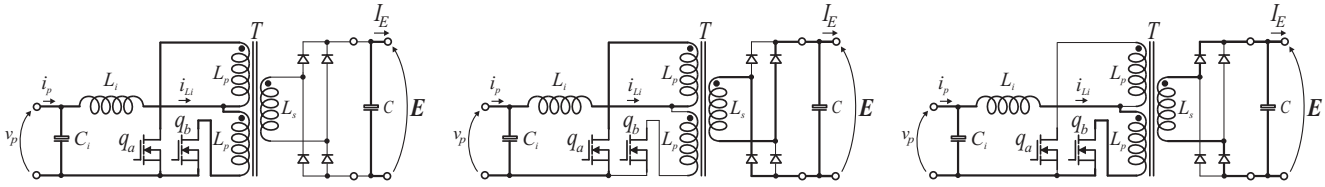

(a) q_a and q_b closed (b) q_a closed and q_b open (c) q_a open and q_b closed

Fig. 5: Converter switching modes

V. *PWM* CONTROL

Considering that the converter reference voltages are v_g^* and v_f^*, so:

$$v_g^* = v_{10}^* + v_{20}^* \quad (12)$$
$$v_f^* = v_{30}^* + v_{40}^* \quad (13)$$

The pulse width of the gate signal can be calculated from the voltage referred to the *DC*-bus midpoint, which is given by the desired converter voltages. If the desired voltages are specified by v_g^* and v_f^*, then the reference midpoint voltages can be expressed as

$$v_{10}^* = v_g^* + v_{\mu_g}^* \quad (14)$$
$$v_{20}^* = v_{\mu_g}^* \quad (15)$$
$$v_{30}^* = v_{\mu_f}^* \quad (16)$$
$$v_{40}^* = v_f^* + v_{\mu_f}^* \quad (17)$$

where: $|v_{10}^*| \leq \frac{E}{2}$ and $|v_{20}^*| \leq \frac{E}{2}$, $|v_{30}^*| \leq \frac{E}{2}$ and $|v_{40}^*| \leq \frac{E}{2}$.

The voltages $v_{\mu_g}^*$ and $v_{\mu_f}^*$ can be calculated taking into account the apportioning factors μ_g and μ_f, that are

$$v_{\mu_g}^* = E(\mu_g - \frac{1}{2}) - \mu_g v_{\max_g}^* + (\mu_g - 1)v_{\min_g}^* \quad (18)$$
$$v_{\mu_f}^* = E(\mu_f - \frac{1}{2}) - \mu_f v_{\max_f}^* + (\mu_f - 1)v_{\min_f}^* \quad (19)$$

where $v_{\max_g}^* = \max V_g$ and $v_{\min_g}^* = \min V_g$ where $V_g = \{v_{10}^*, v_{20}^*\}$ for the converter G and $v_{\max_f}^* = \max V_f$ and $v_{\min_f}^* = \min V_f$ where $V_f = \{v_{30}^*, v_{40}^*\}$ for the converter F.

These expressions were derived using the same approach as used to obtain the equivalent one to for the three-phase PWM modulator [10, 11].

The apportioning factors μ_g ($0 \leq \mu_g \leq 1$) and μ_f ($0 \leq \mu_f \leq 1$) are given by

$$\mu_g = t_{oig}/t_{ol} \quad (20)$$
$$\mu_f = t_{oif}/t_{of} \quad (21)$$

and indicate the distribution of the free-wheeling periods t_{og} and t_{of} (periods in which the voltages $v_{10} = v_{20}$ and $v_{30} = v_{40}$) between the beginning (($t_{oig} = \mu_g t_{og}$) and ($t_{oif} = \mu_f t_{of}$)) and the end (($t_{ofg} = (1 - \mu_g)t_{og}$) and ($t_{off} = (1 - \mu_f)t_{of}$)) of the switching periods [10, 11]. The apportioning factor can be changed as a function of the modulation index to reduce the THD (total harmonic distortion) of both converters voltages [10, 11].

The pulse width of the gating signals can be calculated from the reference pole voltages,

$$\tau_1 = \frac{T}{2} + \frac{T}{E}v_{10}^* \quad (22)$$
$$\tau_2 = \frac{T}{2} + \frac{T}{E}v_{20}^* \quad (23)$$
$$\tau_3 = \frac{T}{2} + \frac{T}{E}v_{30}^* \quad (24)$$
$$\tau_4 = \frac{T}{2} + \frac{T}{E}v_{40}^* \quad (25)$$

The proposed algorithm for this method is:
Step 1. Choose the apportioning factors μ_g and μ_f and, then calculate $v_{\mu_g}^*$ from (18) and $v_{\mu_f}^*$ from (19).
Step 2. Determine the voltages v_{10}^*, v_{20}^*, v_{30}^* and v_{40}^* from (14)-(17).
Step 3. Calculate the pulse widths τ_1, τ_2, τ_3 and τ_4 using (22)-(25).

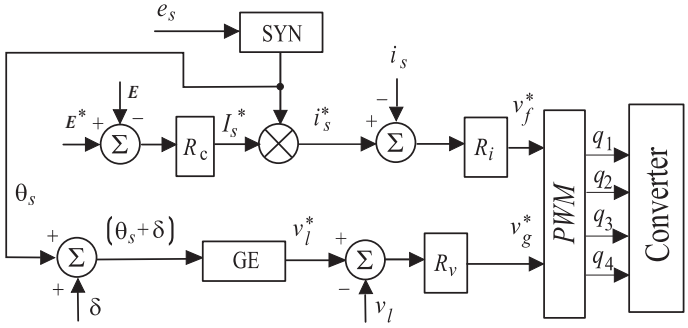

Fig. 6: Block diagram of the control system.

VI. FILTER CONTROL SYSTEM

The block diagram of the control system is given in Fig. 6. In this figure it is observed that the capacitor voltage E is compared to the reference voltage E^* and as result an error is applied to the PI controller, represented by R_c. The output of the controller defines the magnitude of the reference current i_s^* that must be synchronized to the voltage e_s. The current error ($i_s^* - i_s$) is then applied to the PI controller represented by R_i, of which the output voltage v_f^* is used to determine the conduction state of the switches.

The voltage regulation v_g^* is implemented by PI controller, through R_v block. The voltage e_l^* is determined

from $(\theta + \delta)$. θ is the instantaneous angle of e_s and δ is the phase angle. The angle δ is determined as function of the best performance point of the system [12].

VII. SIMULATION RESULTS

In order to analyze the behavior of the system presented in Fig. 1, simulations were made by the use of programs written in C++ and Matlab® and the switching frequencies were 10.0kHz for the inverter and 100kHz for the push-pull.

Some data for the simulated system (Fig. 1) are: load voltage, $e_l^* = 110\sqrt{2}\cos(\omega t)$V, where $\omega = 2\pi 60$; load power, $P_l = 60$W; load power factor, $\cos\theta_l = 0.7$; maximum power of photovoltaic generator, $P_{max}^r = 1.28$kW; DC-bus voltage, $E^* = 350$V; photovoltaic generator with four-series, four-parallel, 80W modules (1280W total).

The simulation helped the analysis of the system behavior under the following conditions: i) the photovoltaic generator supplies more energy than system consumes, ii) the photovoltaic generator supplies part of the energy that the system needs and iii) the photovoltaic generator supplies no energy to the system.

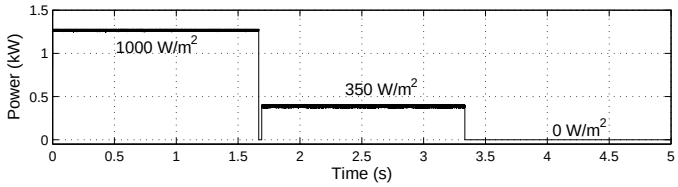

Fig. 7: Power of photovoltaic generator

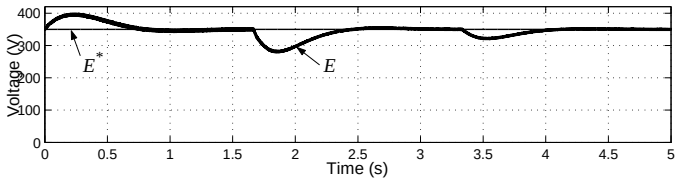

Fig. 8: DC-bus voltage

Figure 7 presents the transient of power to which the photovoltaic generator is submitted due to the insolation variation. It is observed that the MPPT method acts as forcing the generator to operate in MPP. In Fig. 8 it is observed that the voltage controller of the DC-bus regulates the voltage to a pre-defined value. In Fig. 11 is shown the waveform of sinusoidal signals of the system. It is noted that the current i_s in Fig. 11(a) is delayed 180^o from the voltage e_s; this means that the energy flows out of the system to the grid. In this case, the generated energy by the photovoltaic generator was higher than that the system needed. In Fig. 11(b) a fifth harmonic was added to e_s, however, this harmonic component does not appear in the voltage e_l because converter G acted and eliminated this component. In Fig. 11(b) it can also be observed that i_s phase is close to e_s. Finally, in Fig. 11(c) the photovoltaic generator is not delievering any power, because the insolation was 0W/m^2. In this case, the active power filter is responsible only for compensating reactives and harmonic distortions.

VIII. EXPERIMENTAL RESULTS

Experimental results were obtained with the help of a dedicated setup in which an inverter operates with a switching frequency of $10kHz$. Fig. 9 and 10 show the experimental results of the single-phase universal power filter. In Fig. 9, the grid voltage e_s and the grid current i_s indicate a power factor close to unity. Fig. 10 indicates the grid voltage e_s and the voltage applied to the load e_l. In this figure does exist a difference between voltages e_s and e_l in terms of amplitude, showing that the load voltage controller maintained e_l in the desired value even when a sag occurred in the grid.

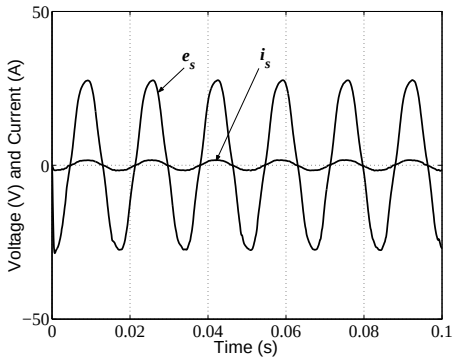

Fig. 9: Power factor control

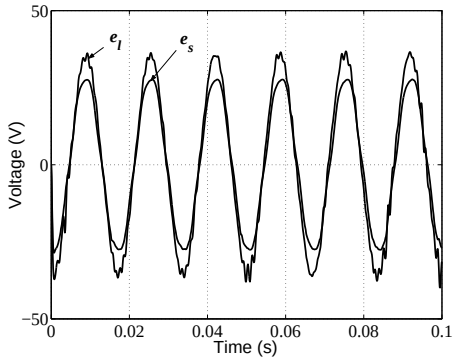

Fig. 10: Grid and load voltages

IX. CONCLUSION

This paper presented the study of the single-phase static universal power filter with photovoltaic co-generation. The following operation conditions were addressed: i) the photovoltaic generator supplies more energy than system consumes, ii) the photovoltaic generator supplies part of the energy that the system needs and iii)

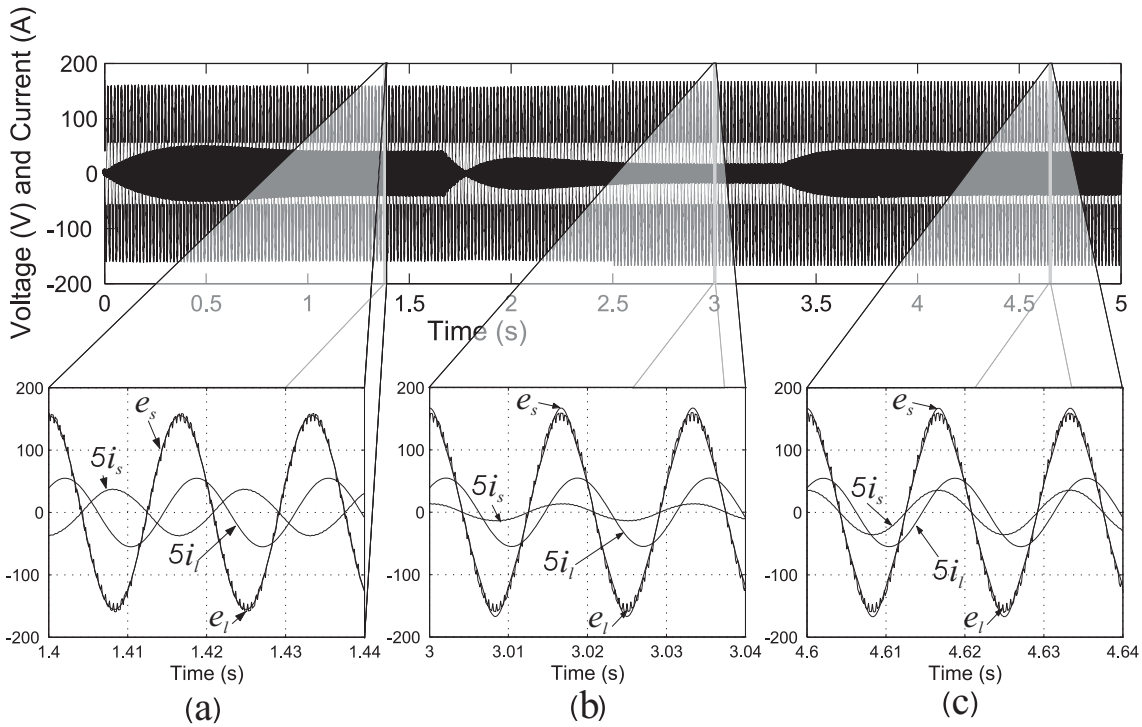

Fig. 11: Simulations results of voltage and current of the system

the photovoltaic generator supplies no energy to the system. In all cases the system presented satisfactory results: power factor close to unity, low current distortion and the output load voltage at desired value.

ACKNOWLEDGEMENT

The authors would like to thank the financial support given by the Conselho Nacional de Desenvolvimento Científico e Tecnológico (CNPq) and the Coordenação de Aperfeiçoamento de Pessoal de Nível Superior (CAPES).

REFERENCES

[1] H. Akagi. Trends in active power line conditioners. *IEEE Trans. Power Electron.*, 9(3):263–268, May 1994.

[2] B. Singh, K. Al-Haddad, and A. Chandra. A review of active filters for power quality improvement. *IEEE Trans. Ind. Electron.*, 46(5):960–971, Oct. 1999.

[3] J. Carey, A. Aston, J. Hibbard, and R. Grover. Alternate power: A change is in the wind. *Business Week Online*, July 2005. Accessible from <`http://www.businessweek.com/magazine/content/05_27/b3941036_mz011.htm`>. Last accessed April 09, 2007.

[4] G. Boyle. *Renewable Energy.* Oxford University Press, 2004.

[5] R. M. G. Castro. Introdução à energia fotovoltaica, energias renováveis e produção descentralizada. Technical report, Instituto Superior Técnico de Lisboa, January 2004.

[6] K. C. Oliveira, M. C. Cavalcanti, G. M. S. Azevedo, and F. A. S. Neves. Comparative study of maximum power point tracking techniques for photovoltaic systems. *Conf. Rec. VII INDUSCON*, pages 1–6, 2006.

[7] M. A. El-Shibini and H. H. Rakha. Maximum power point tracking technique. *MELECON '89*, pages 21–24, April 1989.

[8] K. K. Tse, M. T. Ho, H. S. H. Chung, and S. Y. Hui. A novel maximum power point tracker for pv panels using switching frequency modulation. *Power Electronics, IEEE Transactions on*, 17(06):980 – 989, November 2005.

[9] K.H. Hussein, I. Muta, T. Hoshino, and M. Osakada. Maximum photovoltaic power tracking: an algorithm for rapidly changing atmospheric conditions. *IEE Proc. Gener. Transm. Distrib.*, 142(1):59–64, January 1995.

[10] C. B. Jacobina, A. M. N. Lima, E. R. C. da Silva, R. N. C. Alves, and P. F. Seixas. Digital scalar pulse width modulation: a simple approach to introduce non-sinusoidal modulating waveforms. *IEEE Trans. Power Electron.*, 16(3):351–359, May 2001.

[11] V. Blasko. Analysis of a hybrid pwm based on modified space-vector and triangle-comparison methods. *IEEE Trans. Ind. Applicat.*, 33(3):756–764, May/June 1996.

[12] W. R. N. Santos, C. B. Jacobina, A. C. Oliveira, and E. R. C. Silva. Compensador estático universal para aplicações em sistemas monofásicos. *Congresso Brasileiro de Automática*, pages 3385–3390, Outubro 2006.